Analytic form for a nonlocal kinetic energy functional with a density-dependent kernel for orbital-free density functional theory under periodic and Dirichlet boundary conditions

Gregory S. Ho,[1] Vincent L. Lignères,[1] and Emily A. Carter[2,][*]

[1]*Department of Chemistry, Princeton University, Princeton, New Jersey 08544, USA*
[2]*Department of Mechanical and Aerospace Engineering and Program in Applied and Computational Mathematics,*
Princeton University, Princeton, New Jersey 08544-5263, USA

We derive an analytic form of the Wang-Govind-Carter (WGC) [Wang *et al.*, Phys. Rev. B **60**, 16350 (1999)] kinetic energy density functional (KEDF) with the density-dependent response kernel. A real-space aperiodic implementation of the WGC KEDF is then described and used in linear scaling orbital-free density functional theory (OF-DFT) calculations.

PACS number(s): 71.15.Mb, 71.20.Gj

I. INTRODUCTION

Orbital-free density functional theory (OF-DFT) is a first-principles quantum mechanics method that can be formulated to scale linearly with system size.[1] By contrast, Kohn-Sham density functional theory (KS-DFT) (Ref. 2) scales cubically with size initially and can be made to scale linearly in the asymptotic limit. The linear scaling within OF-DFT is achieved by eliminating the fictitious orbitals employed within KS-DFT, which are invoked to obtain an accurate estimate of the kinetic energy of the electrons. Instead, OF-DFT relies upon explicit functionals of the electron density to compute all energy terms, including the kinetic energy.

OF-DFT is significantly faster than KS-DFT. Currently, OF-DFT can be used to study samples consisting of tens of thousands of atoms on a single processor. Unfortunately, this increase in speed currently comes at a cost in accuracy. The kinetic energy within KS-DFT is exact in the limit of noninteracting electrons, whereas the form of the OF kinetic energy density functional (KEDF) is known exactly only for the uniform electron gas and for a single orbital, and approximations must be used for all other cases.[3] Because of this limitation, OF-DFT is currently only as accurate as KS-DFT for main group metals (~ 10 meV/atom difference),[4] and for some properties of semiconductors.[5]

In most cases, the most accurate KEDF currently available is the Wang-Govind-Carter (WGC) KEDF with the density-dependent response kernel.[4] The WGC KEDF is derived from a class of KEDFs that explicitly account for the linear response of the density of a uniform electron gas subject to small perturbations in the potential. As a result, these KEDFs work best for main group, nearly-free-electron-like metals. This class of KEDF was pioneered by Wang and Teter (WT),[6] modified by Perrot,[7] and Madden and co-workers,[8–10] and generalized by WGC.[11] These KEDFs all rely upon a linear-response kernel derived from a single fixed reference density. However, WGC introduced an important advance by accounting for a nonlocal density dependence in the linear-response kernel.[4] This density dependence significantly improves upon the WT KEDF in many cases, particularly for describing vacancies, surfaces, and equations of state. Some properties of silicon, a representative covalent semiconductor, are also well described using

two slightly different parameters in the 1999 WGC KEDF.[5] However, sufficiently accurate KEDFs have yet to be developed for localized electron densities present in, e.g., transition metals,[12] or molecules.[3] Perhaps unfortunately, the WGC KEDF is still the most accurate KEDF for condensed matter to date.[4]

The kernel of the WGC KEDF is obtained by solving a second-order differential equation described below. Previous implementations of the WGC KEDF used a numerical solution to this differential equation. Here we present an analytic solution, which offers several advantages over the numerical solution, in our new software PROFESS (PRinceton Orbital-Free Electronic Structure Software).[1] First, the kernel can be computed on the fly for any given system using the analytic solution and stored on a grid with the appropriate mesh spacing. A numerical solution inevitably requires interpolation. Second, parameters in the kernel are simple to adjust in the analytic solution, requiring no extra effort. In a numerical implementation, one has to compute and store a different solution for every set of parameters. Third, knowledge of the analytic solution, which has not been reported previously, makes it possible to derive the WGC KEDF in real space, in order to perform accurate OF-DFT calculations under Dirichlet (fixed) boundary conditions as opposed to periodic boundary conditions (PBCs). Dirichlet boundary conditions allow the study of aperiodic or isolated systems, such as a dislocation, grain boundary, or crack in a bulk material or a nanostructure (e.g., quantum dot or wire), without periodic image artifacts inherent with periodic boundary conditions.

In what follows, we first derive the analytic form of the kernel used in the WGC KEDF. With this in hand, we present our implementation of the WGC KEDF under Dirichlet boundary conditions, which maintains near-linear $O(N \ln N)$ scaling of the computation time with respect to system size. We validate our approach on the following test cases: a single aluminum atom in a vacuum, a cluster of 14 aluminum atoms in vacuum, and a cluster of 108 aluminum atoms arranged in a face-centered-cubic orientation without vacuum, but with the values of the electron density at the boundaries specified to be the same as in bulk fcc aluminum.

II. ANALYTIC FORM OF THE WGC KEDF

The linear-response term in the WGC KEDF with the density-dependent kernel can be written as[4]

$$T_{\text{WGC}}^{\alpha,\beta,\gamma}[\rho] = C_{\text{TF}}\langle \rho^{\alpha}(\vec{r})|w_{\alpha,\beta}(\xi_{\gamma}(\vec{r},\vec{r}'),\vec{r}-\vec{r}')|\rho^{\beta}(\vec{r}')\rangle, \quad (1)$$

where $C_{\text{TF}} = \frac{3}{10}(3\pi^2)^{1/3}$, $w_{\alpha,\beta}$ is the WGC kernel in real space, and

$$\xi_{\gamma}(\vec{r},\vec{r}') = \left[\frac{k_F^{\gamma}(\vec{r}) + k_F^{\gamma}(\vec{r}')}{2}\right]^{1/\gamma} \quad (2)$$

is a nonlocal two-body Fermi wave vector, and $k_F(\vec{r}) = [3\pi^2\rho(\vec{r})]^{1/3}$ is the local one-body Fermi wave vector. The set of parameters (α,β,γ) can be adjusted to optimize the performance of the functional, and the best choices are somewhat dependent on the identities of the atoms in the system. Universal values of α and β have been derived by asymptotic analysis, based on linear-response theory applied to the uniform electron gas.[4,11]

Unfortunately, Eq. (1) contains density-dependent terms in the kernel, and straightforward application of the convolution theorem using fast Fourier transforms to achieve linear scaling is not possible. However, Wang *et al.*[4] showed that the density dependence may be factored out using a Taylor series expansion. As long as the electron density in the system is sufficiently close to the reference density employed, the Taylor expansion is a good approximation to the WGC kernel. Since the explicit density dependence is factored out of the kernel by use of this Taylor expansion around a constant reference density, the convolution theorem can be used again, allowing quasilinear scaling. Unfortunately, this expansion can be carried out to only second order, because higher-order terms (involving the third and higher derivatives of the kernel) diverge due to the logarithmic singularity of the Lindhard function[13] from which the WGC kernel is derived.[4]

By enforcing the exact linear response at the uniform electron-gas limit,[4] one finds that $w_{\alpha,\beta}(\xi_{\gamma}(\vec{r},\vec{r}'),\vec{r}-\vec{r}')$ is given by the solution of the following universal second-order differential equation in reciprocal space for every value of $\vec{q}$:

$$|\vec{\eta}|^2\tilde{w}''_{\alpha,\beta,\gamma}(\vec{\eta},\rho_0) + [\gamma + 1 - 6(\alpha+\beta)]|\vec{\eta}|\tilde{w}'_{\alpha,\beta,\gamma}(\vec{\eta},\rho_0)$$
$$+ 36\alpha\beta\tilde{w}_{\alpha,\beta,\gamma}(\vec{\eta},\rho_0) = 20G(\vec{\eta})\rho_0^{5/3-(\alpha+\beta)}, \quad (3)$$

where $\vec{\eta} = \vec{q}/2k_F$, $\vec{q}$ is the momentum, $\tilde{w}_{\alpha,\beta,\gamma}$ is the Fourier transform of the kernel $w_{\alpha,\beta}$ for a uniform density ρ_0, $\tilde{w}'_{\alpha,\beta,\gamma}$ and $\tilde{w}''_{\alpha,\beta,\gamma}$ are its first and second derivatives with respect to $|\vec{\eta}|$, respectively, ρ_0 is the system's average electron density, and the expression for $G(\eta)$ is given elsewhere.[4] Once the solution to Eq. (3) is obtained, the Taylor expansion can be evaluated using previously reported identities.[4]

Again, although $\tilde{w}_{\alpha,\beta,\gamma}$ and its derivatives can be solved numerically, a new numerical solution would have to be obtained every time the parameters α, β, or γ are changed. In addition, a numerical solution that is expressed at fixed values of $\vec{\eta}$ and then read from a file may suffer from interpolation errors if the numerical solution is not dense enough in $\vec{\eta}$. Thus, it is desirable to compute $\tilde{w}_{\alpha,\beta,\gamma}$ analytically.

The analytic solution to the differential equation shown in Eq. (3) can be written as

$$\tilde{w}_{\alpha,\beta,\gamma}(\vec{\eta},\rho_0) = H(\vec{\eta},\rho_0) + P(\vec{\eta},\rho_0), \quad (4)$$

where $H(\vec{\eta})$ is the homogenous solution and $P(\vec{\eta})$ is the particular solution.

It can be shown that the homogenous solution has the form

$$H(\vec{\eta},\rho_0) = \begin{cases} C_1|\vec{\eta}|^{u+\sqrt{v}} + C_2|\vec{\eta}|^{u-\sqrt{v}}, & v > 0 \\ |\vec{\eta}|^u(C_2\ln|\vec{\eta}| + C_1), & v = 0 \\ |\vec{\eta}|^u[C_1\cos(\sqrt{-v}\ln|\vec{\eta}|) + C_2\sin(\sqrt{-v}\ln|\vec{\eta}|)], & v < 0, \end{cases} \quad (5)$$

where

$$C_1 = \begin{cases} 0, & u > 0 \text{ and } |\vec{\eta}| > 1 \\ 0, & u < 0 \text{ and } |\vec{\eta}| < 1; \\ c_1 & \text{otherwise}, \end{cases} \quad c_1 = \begin{cases} \dfrac{u}{|u|}((\sqrt{v}-u)S_d + S_s), & v > 0 \\ \dfrac{u}{|u|}S_d, & v \leq 0, \end{cases}$$

$$C_2 = \begin{cases} 0, & u > 0 \text{ and } |\vec{\eta}| > 1 \\ 0, & u < 0 \text{ and } |\vec{\eta}| < 1; \\ c_2 & \text{otherwise}, \end{cases} \quad c_2 = \begin{cases} \dfrac{u}{|u|}\dfrac{1}{2\sqrt{v}}[(\sqrt{v}+u)S_d - S_s], & v > 0 \\ \dfrac{u}{|u|}(S_s - uS_d), & v = 0 \\ \dfrac{u}{|u|}\dfrac{1}{\sqrt{-v}}(S_s - uS_d), & v < 0, \end{cases} \quad (6)$$

$$S_d = \sum_{i=0}^{\infty}\left[\frac{\Gamma A_i}{(u+2i)^2 - v} - \frac{\Gamma B_i}{(u-2i)^2 - v}\right], \quad (7)$$

$$S_s = \sum_{i=1}^{\infty} \left[\frac{-2i\Gamma A_i}{(u+2i)^2 - v} - \frac{2i\Gamma B_i}{(u-2i)^2 - v} \right], \tag{8}$$

and

$$A_i = \begin{cases} 0, & i = -1 \\ a_0 - 1, & i = 0 \\ a_i, & i > 0, \end{cases} \quad \text{and} \quad a_i = \begin{cases} 3, & i = -1 \\ -3 \left[\sum_{j=-1}^{i-1} \frac{a_j}{4(i-j+1)^2 - 1} \right], & i > -1, \end{cases} \tag{9}$$

$$B_i = \begin{cases} 0, & i = 0 \\ b_1 - 3, & i = 1 \\ b_i, & i > 1, \end{cases} \quad \text{and} \quad b_i = \begin{cases} 1, & i = 0 \\ \sum_{j=0}^{i-1} \frac{b_j}{4(i-j)^2 - 1}, & i > 0. \end{cases} \tag{10}$$

Here,

$$u = 3(\alpha + \beta) - \frac{\gamma}{2}, \tag{11}$$

$$v = u^2 - 36\alpha\beta, \tag{12}$$

and

$$\Gamma = 20\rho_0^{5/3 - (\alpha+\beta)} \tag{13}$$

are constants that depend only on the value of the parameters (α, β, γ).

The form of the particular solution depends on the value of $|\vec{\eta}|$ as follows:

$$P(\vec{\eta}, \rho_0) = \begin{cases} \Gamma \sum_{i=1}^{\infty} \frac{B_i |\vec{\eta}|^{2i}}{(u-2i)^2 - v}, & |\vec{\eta}| < 1 \\ \Gamma \sum_{i=0}^{\infty} \frac{A_i |\vec{\eta}|^{-2i}}{(u+2i)^2 - v}, & |\vec{\eta}| > 1, \end{cases} \tag{14}$$

This analytic form of the WGC kernel in reciprocal space and its analytic derivatives with respect to $|\vec{\eta}|$ are displayed in Fig. 1. The kernel is normalized to zero at $|\vec{\eta}| = 0$ and its asymptotic limit at large $|\vec{\eta}|$ is $-8/5$. The logarithmic singularity in the Lindhard response function at $|\vec{\eta}| = 1$ is visible in the discontinuous behavior of the second derivative function $\tilde{v}_{\alpha,\beta,\gamma}$. This discontinuity makes it impossible to extend the Taylor expansion of the kernel beyond second order.

III. WGC KEDF UNDER DIRICHLET BOUNDARY CONDITIONS

Under periodic boundary conditions (and using the Taylor expansion), the convolution theorem can be used to evaluate Eq. (1). Therefore, $\tilde{w}_{\alpha,\beta,\gamma}$ and its derivatives are needed only in reciprocal space and need never be obtained in real space. However, an extra step is needed in order to evaluate the WGC KEDF [Eq. (1)] within Dirichlet boundary conditions. Instead of using standard convolutions, a real-space convolution (also known as the Hockney method) must be used.[14,15] Since the real-space convolution requires one to start with the kernel in real space and then to construct a circulant kernel based on it, the WGC kernel and its derivatives with respect to $|\vec{\eta}|$ must be obtained in real space. A variation of the strategy detailed in Ref. 14 that was used to transform the density-independent Wang-Teter kernel[16] into real space can be adapted to do this. We describe the method in detail here as it pertains to the WGC kernel.

In principle, the Fourier-Bessel transform should be used to obtain the kernel in real space,

$$w_{\alpha,\beta,\gamma}(\vec{r} - \vec{r}', \rho_0) = \frac{1}{2\pi^2} \int_0^{\infty} \tilde{w}_{\alpha,\beta,\gamma}(\vec{\eta}, \rho_0) |\vec{q}|^2 \frac{\sin(|\vec{q}||\vec{r} - \vec{r}'|)}{|\vec{q}||\vec{r} - \vec{r}'|} d|\vec{q}|. \tag{15}$$

However, since the WGC kernel dies off as $1/|\vec{\eta}|^2$ as $|\vec{\eta}| \to \infty$, the integrand here is long ranged. Therefore, this trans-

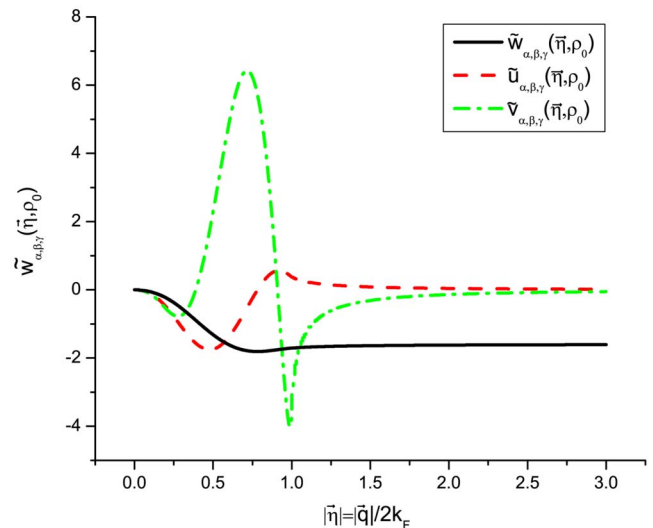FIG. 1. (Color online) The analytic Wang-Govind-Carter kernel $\tilde{w}_{\alpha,\beta,\gamma}(\vec{\eta}, \rho_0)$ [Eqs. (4)–(14)] and its derivatives $\tilde{u}_{\alpha,\beta,\gamma}(\vec{\eta}, \rho_0) = |\vec{\eta}| \tilde{w}'_{\alpha,\beta,\gamma}(\vec{\eta}, \rho_0)$ and $\tilde{v}_{\alpha,\beta,\gamma}(\vec{\eta}, \rho_0) = |\vec{\eta}|^2 \tilde{w}''_{\alpha,\beta,\gamma}(\vec{\eta}, \rho_0)$ for $\rho_0 = 0.183/\text{Å}^3$, $(\alpha, \beta) = 5/6 \pm \sqrt{5}/6$, and $\gamma = 2.7$.

form is difficult to perform in a straightforward fashion. Instead, it is convenient to break up the kernel into three parts,

$$\widetilde{w}_{\alpha,\beta,\gamma}(\vec{\eta},\rho_0) = \widetilde{w}_{\alpha,\beta,\gamma}^{\mathrm{I}}(\vec{\eta},\rho_0) + \widetilde{w}_{\alpha,\beta,\gamma}^{\mathrm{II}}(\vec{\eta},\rho_0) + \widetilde{w}_{\alpha,\beta,\gamma}^{\mathrm{III}}. \quad (16)$$

Here $\widetilde{w}_{\alpha,\beta,\gamma}^{\mathrm{II}}(\vec{\eta},\rho_0)$ approximates the asymptotic behavior of the kernel with an analytic function (within an additive constant $\widetilde{w}_{\alpha,\beta,\gamma}^{\mathrm{III}}$), which can be transformed analytically. The transform of the constant $\widetilde{w}_{\alpha,\beta,\gamma}^{\mathrm{III}}$ is simply $\delta(\vec{r}-\vec{r}')w_{\alpha,\beta,\gamma}^{\mathrm{III}}$ where $\delta(\vec{r}-\vec{r}')$ is the Dirac delta function. The remaining part $\widetilde{w}_{\alpha,\beta,\gamma}^{\mathrm{I}}(\vec{\eta},\rho_0)$ will be short ranged in $\vec{\eta}$, and therefore is easy to transform numerically.

We first fit the long-range behavior of $\widetilde{w}_{\alpha,\beta,\gamma}$ to the function

$$\widetilde{w}_{\alpha,\beta,\gamma}^{\mathrm{II}}(\vec{\eta}) = \frac{A|\vec{\eta}|^2}{|\vec{\eta}|^4 + B|\vec{\eta}|^2 + B^2}, \quad (17)$$

where A and B are constants to be determined. In order to do this, the long-range behavior of $\widetilde{w}_{\alpha,\beta,\gamma}$ in Eq. (4) must first be analyzed. As $|\vec{\eta}| \to \infty$,

$$\widetilde{w}_{\alpha,\beta,\gamma} \to \Gamma \sum_{i=0}^{\infty} \frac{A_i|\vec{\eta}|^{-2i}}{(u+2i)^2 - v} + H(\vec{\eta}). \quad (18)$$

Two possible cases exist: $u > 0$ and $u \leq 0$. However, when $u > 0$ and $|\vec{\eta}| \to \infty$, $C_1 = C_2 = 0$ and $H(\vec{\eta}) = 0$ [Eqs. (5) and (6)]. This simplifies considerably the rest of our analysis for the $u > 0$ case, which thus can be written as

$$\widetilde{w}_{\alpha,\beta,\gamma} \to \Gamma \sum_{i=0}^{\infty} \frac{A_i|\vec{\eta}|^{-2i}}{(u+2i)^2 - v}, \quad u > 0. \quad (19)$$

Fortunately, one constraint on the values of α and β is that $\alpha + \beta = \frac{5}{3}$, which is meant to ensure that the total kinetic energy functional reduces to the correct large-$\vec{q}$ limit.[4] By imposing this constraint, Eq. (11) implies that $u \leq 0$ only if $\gamma \geq 10$. However, optimal values of γ for real materials have been determined to be much smaller than 10 [for Al and Si, $\gamma = 2.7$ and 3.6 are optimum, respectively,[4,5] although there is recent evidence that $\gamma = 4.2$ may in fact be a superior choice for Si (Ref. [17])]. Therefore, for simplicity, throughout the rest of this paper we will assume that $u > 0$. Extension of the method to cases where $u \leq 0$ is a straightforward but somewhat tedious endeavor.

Writing out the terms from Eq. (19) as $|\vec{\eta}| \to \infty$,

$$\widetilde{w}_{\alpha,\beta,\gamma} \to \frac{\Gamma A_0}{u^2 - v} + \frac{\Gamma A_1}{(u+2)^2 - v}\left(\frac{1}{|\vec{\eta}|^2}\right) + \frac{\Gamma A_2}{(u+4)^2 - v}\left(\frac{1}{|\vec{\eta}|^4}\right)$$

$$+ O\left(< \frac{1}{|\vec{\eta}|^4}\right). \quad (20)$$

Carrying out long division in Eq. (17) and matching terms of the same order in $|\vec{\eta}|$, appropriate values for $\widetilde{w}_{\alpha,\beta,\gamma}^{\mathrm{III}}$, A, and B are determined to be

$$\widetilde{w}_{\alpha,\beta,\gamma}^{\mathrm{III}} = \frac{\Gamma A_0}{u^2 - v}, \quad A = \frac{\Gamma A_1}{(u+2)^2 - v}, \quad B = -\frac{\Gamma A_2[(u+2)^2 - v]}{A_1[(u+4)^2 - v]}. \quad (21)$$

The three panels of Fig. 2 show that the asymptotic behavior of $\widetilde{w}_{\alpha,\beta,\gamma}$ and its derivatives is indeed captured successfully with $\widetilde{w}_{\alpha,\beta,\gamma}^{\mathrm{II}}(\vec{\eta},\rho_0)$ and $\widetilde{w}_{\alpha,\beta,\gamma}^{\mathrm{III}}$ using the above parameters.

$\widetilde{w}_{\alpha,\beta,\gamma}^{\mathrm{I}}(\vec{\eta},\rho_0)$ is then obtained numerically from

$$\widetilde{w}_{\alpha,\beta,\gamma}^{\mathrm{I}}(\vec{\eta},\rho_0) = \widetilde{w}_{\alpha,\beta,\gamma}(\vec{\eta},\rho_0) - \widetilde{w}_{\alpha,\beta,\gamma}^{\mathrm{II}}(\vec{\eta},\rho_0) - \widetilde{w}_{\alpha,\beta,\gamma}^{\mathrm{III}}, \quad (22)$$

where $\widetilde{w}_{\alpha,\beta,\gamma}(\vec{\eta},\rho_0)$ is derived analytically via Eq. (4).

At this point, the kernel $\widetilde{w}_{\alpha,\beta,\gamma}(\vec{\eta},\rho_0)$ has been decomposed into components as in Eq. (16). To obtain the transform of $\widetilde{w}_{\alpha,\beta,\gamma}(\vec{\eta},\rho_0)$ into real space, we simply transform each component individually. Although the goal is to eventually obtain the transform from $|\vec{q}|$ space to $|\vec{r}-\vec{r}'|$ space, it is convenient to first perform the transform from $|\vec{\eta}|$ space to $|\vec{\lambda}|$ space, where $\vec{\lambda} = 2k_F(\vec{r}-\vec{r}')$ is a dimensionless length in real space, in order to simplify bookkeeping during the analytical transform of Eq. (17). Then, a change of variables can be performed to obtain the result of the transform from $|\vec{q}|$ space to $|\vec{r}-\vec{r}'|$ space.

We use a Fourier-Bessel transform to take $\widetilde{w}_{\alpha,\beta,\gamma}^{\mathrm{I}}(\vec{\eta},\rho_0)$ numerically from $|\vec{\eta}|$ space to $|\vec{\lambda}|$ space to obtain $w_{\alpha,\beta,\gamma}^{\mathrm{I}}(\vec{\lambda},\rho_0)$. Figure 3 displays the transformed kernel $w_{\alpha,\beta,\gamma}^{\mathrm{I}}(\vec{\lambda},\rho_0)$ and its derivatives as a function of the dimensionless real-space variable $|\vec{\lambda}|$. $w_{\alpha,\beta,\gamma}^{\mathrm{I}}(\vec{\lambda},\rho_0)$ is smooth and fairly short ranged compared to its second derivative, which is long ranged and oscillatory.

$\widetilde{w}_{\alpha,\beta,\gamma}^{\mathrm{II}}(\vec{\eta},\rho_0)$ can be transformed analytically from $|\vec{\eta}|$ space to $|\vec{\lambda}|$ space via the residue theorem[18] to obtain[14]

$$w_{\alpha,\beta,\gamma}^{\mathrm{II}}(\vec{\lambda},\rho_0) = \frac{A}{4\pi} \frac{1}{|\vec{\lambda}|} e^{-|\vec{\lambda}|\sqrt{|B|}/2} \left[\frac{\cos(\sqrt{3}\sqrt{|B|}|\vec{\lambda}|)}{2} + \frac{\sqrt{3}}{3} \frac{\sin(\sqrt{3}\sqrt{|B|}|\vec{\lambda}|)}{2} \right]. \quad (23)$$

The transform of $\widetilde{w}_{\alpha,\beta,\gamma}^{\mathrm{II}}(\vec{\eta},\rho_0)$ (as well as its derivatives with respect to $|\vec{\eta}|$) is displayed in Fig. 4. Note that the transformed kernel diverges at small $|\vec{\lambda}|$, but dies off very quickly as $|\vec{\lambda}|$ increases.
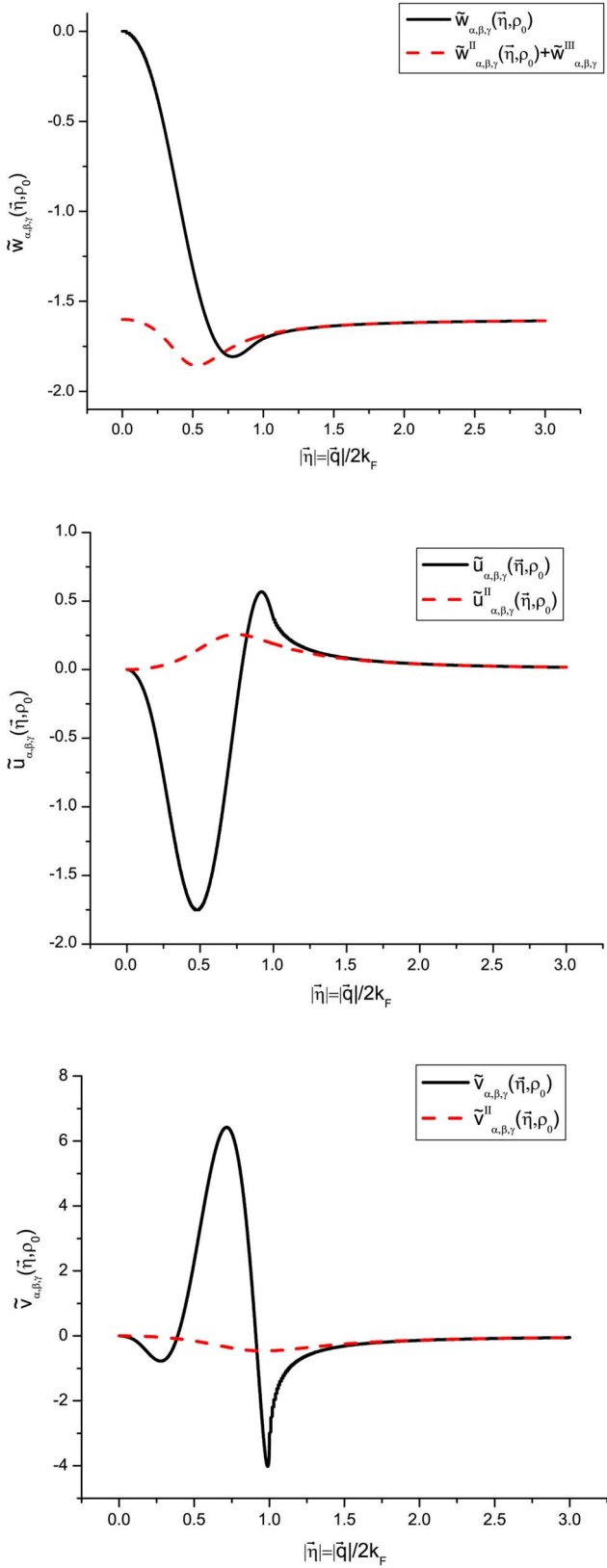
FIG. 2. (Color online) Plots of a function $\tilde{w}^{II}_{\alpha,\beta,\gamma}(\vec{\eta},\rho_0)$ [Eq. (17)] designed to capture the decay of the WGC kernel and its derivatives (dashed) overlaid on the WGC kernel [Eqs. (4)–(14)] and its derivatives (solid).
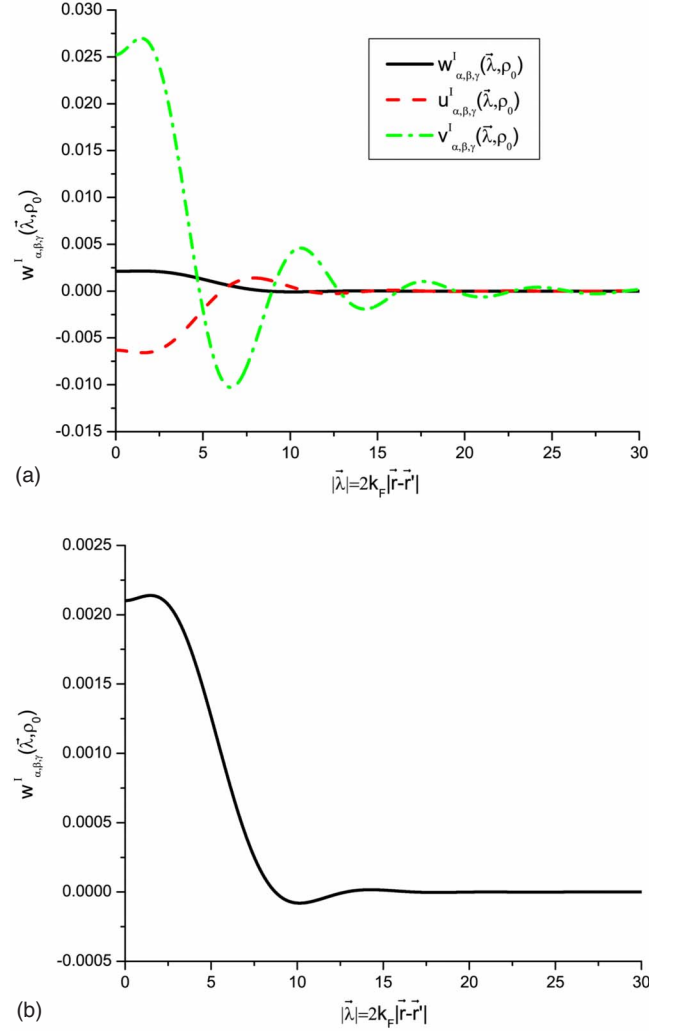

FIG. 3. (Color online) Fourier transform to $|\vec{\lambda}|$ space of the short-range component [originally in $|\vec{\eta}|$ space, Eq. (22)] of the kernel for the WGC KEDF. These parts of the kernel are Fourier transformed numerically. (a) $w^{I}_{\alpha,\beta,\gamma}(\vec{\lambda},\rho_0)$, $u^{I}_{\alpha,\beta,\gamma}(\vec{\lambda},\rho_0)$, and $v^{I}_{\alpha,\beta,\gamma}(\vec{\lambda},\rho_0)$. (b) Blowup of $w^{I}_{\alpha,\beta,\gamma}(\vec{\lambda},\rho_0)$.

The singularity in $w^{II}_{\alpha,\beta}(\vec{\lambda},\rho_0)$ as $|\vec{\lambda}| \rightarrow 0$ can cause numerical instabilities. This can be circumvented by adding and subtracting a factor of $1/|\vec{\lambda}|$,[14]

$$w^{II}_{\alpha,\beta,\gamma}(\vec{\lambda},\rho_0) = \left(\frac{A}{4\pi}\frac{1}{|\vec{\lambda}|}\right) + \frac{A}{4\pi}\frac{1}{|\vec{\lambda}|}\left\{e^{-|\vec{\lambda}|\sqrt{|B|}/2}\left[\frac{\cos(\sqrt{3}\sqrt{|B|}|\vec{\lambda}|)}{2}\right.\right.$$
$$\left.\left. + \frac{\sqrt{3}}{3}\frac{\sin(\sqrt{3}\sqrt{|B|}|\vec{\lambda}|)}{2}\right] - 1\right\}. \quad (24)$$

The first term (a simple $1/|\vec{\lambda}|$ interaction) then can be treated as a multiple of the Coulomb kernel and now the second term no longer contains the singularity.

Putting it all together, the complete expression for the kernel of the WGC functional in real space is
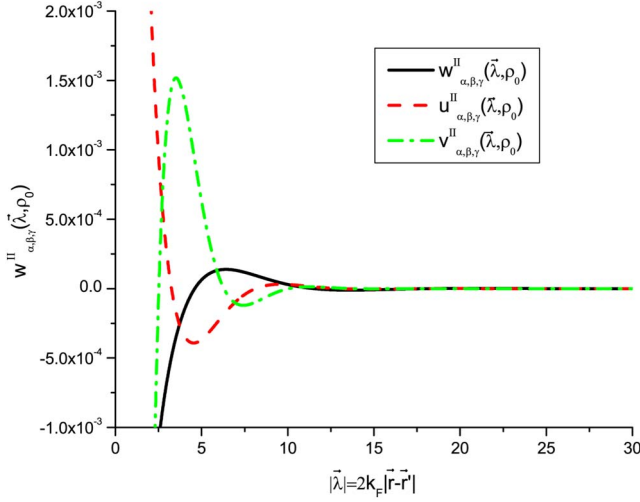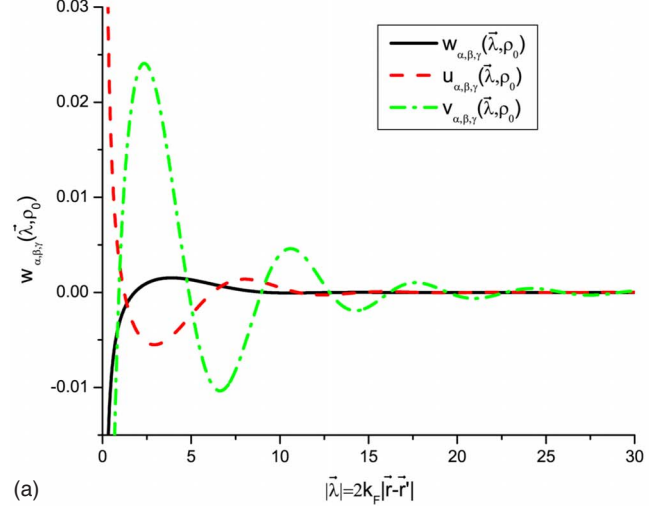
FIG. 4. (Color online) Fourier transform to $|\vec{\lambda}|$ space of the long-range components (originally in $|\vec{\eta}|$ space) of the kernel for the WGC KEDF [Eq. (23)]. $w_{\alpha,\beta,\gamma}^{II}(\vec{\lambda},\rho_0)$, $u_{\alpha,\beta,\gamma}^{II}(\vec{\lambda},\rho_0)$, and $v_{\alpha,\beta,\gamma}^{II}(\vec{\lambda},\rho_0)$ are displayed; these parts of the kernel are transformed analytically.
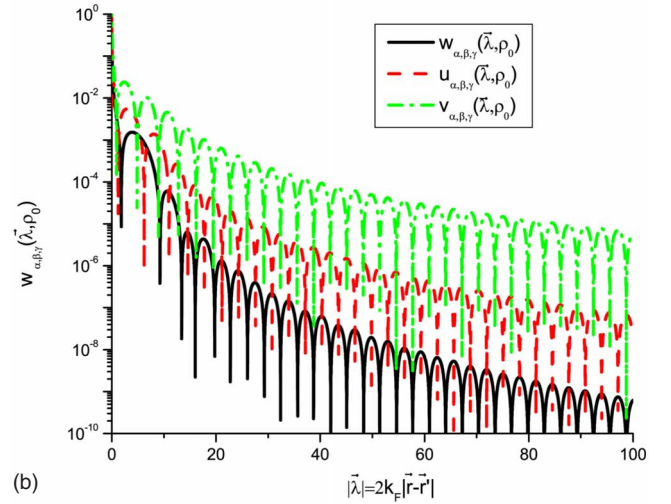
$$
w_{\alpha,\beta,\gamma}(\vec{\lambda},\rho_0) = w_{\alpha,\beta,\gamma}^{I}(\vec{\lambda},\rho_0) + \left(\frac{A}{4\pi}\frac{1}{|\vec{\lambda}|}\right) + \frac{A}{4\pi}\frac{1}{|\vec{\lambda}|}
$$
$$
\times \left\{ e^{-|\vec{\lambda}|\sqrt{|B|}/2}\left[\frac{\cos(\sqrt{3}\sqrt{|B|}|\vec{\lambda}|)}{2} \right.\right.
$$
$$
\left.\left. + \frac{\sqrt{3}}{3}\frac{\sin(\sqrt{3}\sqrt{|B|}|\vec{\lambda}|)}{2} \right] - 1 \right\} + \frac{\Gamma A_0}{u^2 - v}\delta(\vec{\lambda}),
$$
$$(25)$$

where δ is the Dirac delta function. As expected, the kernel and its derivatives diverge at small $|\vec{\lambda}|$ and are oscillatory at long range (Fig. 5). With the Fourier-Bessel transform of $\tilde{w}_{\alpha,\beta,\gamma}$ from $|\vec{\eta}|$ to $|\vec{\lambda}|$ in hand, it is straightforward to transform $\tilde{w}_{\alpha,\beta,\gamma}$ from $|\vec{q}|$ to $|\vec{r}-\vec{r}'|$ in order to obtain $w_{\alpha,\beta,\gamma}(\vec{r}-\vec{r}')$. This is done with a simple change of variables from Eq. (25) as follows:

$$
w_{\alpha,\beta,\gamma}(\vec{r}-\vec{r}',\rho_0) = (2k_F)^3 w_{\alpha,\beta,\gamma}^{I}[2k_F(\vec{r}-\vec{r}'),\rho_0] + \frac{Ak_F^2}{\pi|\vec{r}-\vec{r}'|}
$$
$$
+ \frac{Ak_F^2}{\pi|\vec{r}-\vec{r}'|} \times \left\{ e^{-k_F|\vec{r}-\vec{r}'|\sqrt{|B|}} \right.
$$
$$
\times \left[\frac{\cos(2\sqrt{3}k_F\sqrt{|B|}|\vec{r}-\vec{r}'|)}{2} \right.
$$
$$
\left.\left. + \frac{\sqrt{3}}{3}\frac{\sin(2\sqrt{3}k_F\sqrt{|B|}|\vec{r}-\vec{r}'|)}{2} \right] - 1 \right\}
$$
$$
+ \frac{\Gamma A_0}{u^2 - v}\delta(\vec{r}-\vec{r}').
$$
$$(26)$$

FIG. 5. (Color online) (a) Total $w_{\alpha,\beta,\gamma}(\vec{\lambda},\rho_0)$, $u_{\alpha,\beta,\gamma}(\vec{\lambda},\rho_0)$, and $v_{\alpha,\beta,\gamma}(\vec{\lambda},\rho_0)$. (b) Semilogarithmic plot of the absolute values of total $w_{\alpha,\beta,\gamma}(\vec{\lambda},\rho_0)$, $u_{\alpha,\beta,\gamma}(\vec{\lambda},\rho_0)$, and $v_{\alpha,\beta,\gamma}(\vec{\lambda},\rho_0)$, showing the rate of decay of the long-range oscillations.

Finally, if $\tilde{u}_{\alpha,\beta,\gamma}(\vec{\eta},\rho_0) = |\vec{\eta}|\tilde{w}_{\alpha,\beta,\gamma}'(\vec{\eta},\rho_0)$ and $\tilde{v}_{\alpha,\beta,\gamma}(\vec{\eta},\rho_0) = |\vec{\eta}|^2\tilde{w}_{\alpha,\beta,\gamma}''(\vec{\eta},\rho_0)$, one may obtain $u_{\alpha,\beta,\gamma}(\vec{r}-\vec{r}',\rho_0)$ and $v_{\alpha,\beta,\gamma}(\vec{r}-\vec{r}',\rho_0)$ by taking derivatives of Eq. (20) and repeating the above analysis using the variables u and v in place of w. One finds that both of these expressions take the form of Eq. (26), the only difference being in the values of A and B. For $u_{\alpha,\beta,\gamma}(\vec{r}-\vec{r}',\rho_0)$, one simply substitutes A' for A and B' for B, where $A' = -2A$ and $B' = 2B$. For $v_{\alpha,\beta,\gamma}(\vec{r}-\vec{r}',\rho_0)$, one substitutes A'' for A and B'' for B, where $A'' = 6A$ and $B'' = \frac{10}{3}B$.

IV. RESULTS

We first examine a system consisting of a single aluminum atom under free space boundary conditions (Dirichlet boundary conditions with the value of the electron density at the boundaries specified to be zero) using the local-density approximation (LDA) exchange-correlation functional,[19,20]

sixth-order discretization of the von Weiszäcker (vW) KEDF,[21] and the WGC KEDF with the parameters α, β, and γ set to the previously determined optimal values for bulk fcc Al: $\{\alpha, \beta\} = (5 \pm \sqrt{5})/6$; $\gamma = 2.7$.[4] Since the Goodwin pseudopotential used for aluminum was parameterized on bulk Al, using it for an isolated atom is not scientifically valid. However, it is a useful numerical test. A minimum of 7.5 Å of vacuum on each side of the atom is required to converge the energy to within 1 meV/atom. A grid point density of 13 grid points/Å on each side is also required to converge the energy to within 1 meV/atom.

After electron density optimization using the truncated Newton method, the total energy for the isolated atom under Dirichlet boundary conditions was −55.757 eV/atom. When the same system (using the same grid point density) was optimized under PBCs, a total energy of −55.740 eV/atom was obtained (a 0.02 eV/atom difference).

Next, we examine a cluster of 14 aluminum atoms arranged in an fcc configuration within a cube of dimensions $4.032 \times 4.032 \times 4.032$ Å^3. The cluster is then suspended in vacuum. At least 7.5 Å of vacuum from each face of the cluster to the boundary is needed to converge the total energy to 1 meV/atom. A grid point density of 13 grid points/Å on each side again is required to converge the energy to within 1 meV/atom. Under Dirichlet boundary conditions, density optimization results in a total energy of −57.167 eV/atom. The identical system under PBCs yields an energy of −57.143 eV/atom, which is again a 0.02 eV/atom difference. The 0.02 eV/atom difference simply may be due to image effects remaining in the PBC case.

Finally, we turn our attention to a cubic cluster of 108 aluminum atoms arranged in an fcc configuration with a lattice constant of 4.032 Å. Here we wish to emulate a bulklike environment for the cluster. To this end, we use as an initial guess an optimized electron density associated with periodic bulk fcc Al, shown in Fig. 6(a). Then, having fixed the electron density at the boundary to these bulk values, we optimize the electron density in the interior of the cell subject to these Dirichlet boundary conditions. The fully optimized density is shown in Fig. 6(b). Eventually, if PROFESS is to be used as part of a multiscale model, these boundary conditions may be passed down from a larger length scale calculation. Figure 6 displays the initial guess density described above and the optimized electron density from a cut through an atomic plane in the center of the 108-atom cluster. Due to possible artifacts in fourth- and sixth-order discretization,[21] we use second-order discretization for the vW KEDF. These artifacts may be due to the asymmetric stencils used in the fourth- and sixth-order discretization of the Laplacian operator. If so, this problem can be overcome by simply adding more layers of fixed boundary values of the electron density around the system, which will allow centered stencils always to be used for higher-order discretization.

The difference between the periodic bulk density in Fig. 6(a) and the optimized density in Fig. 6(b) is shown in Fig. 6(c). It is evident that the optimized electron density around the interior atoms is essentially identical to the shape of the electron density around the atoms in the bulk crystal. Only the first layer of atoms at the border shows a significant local perturbation of the electron density. This suggests that the
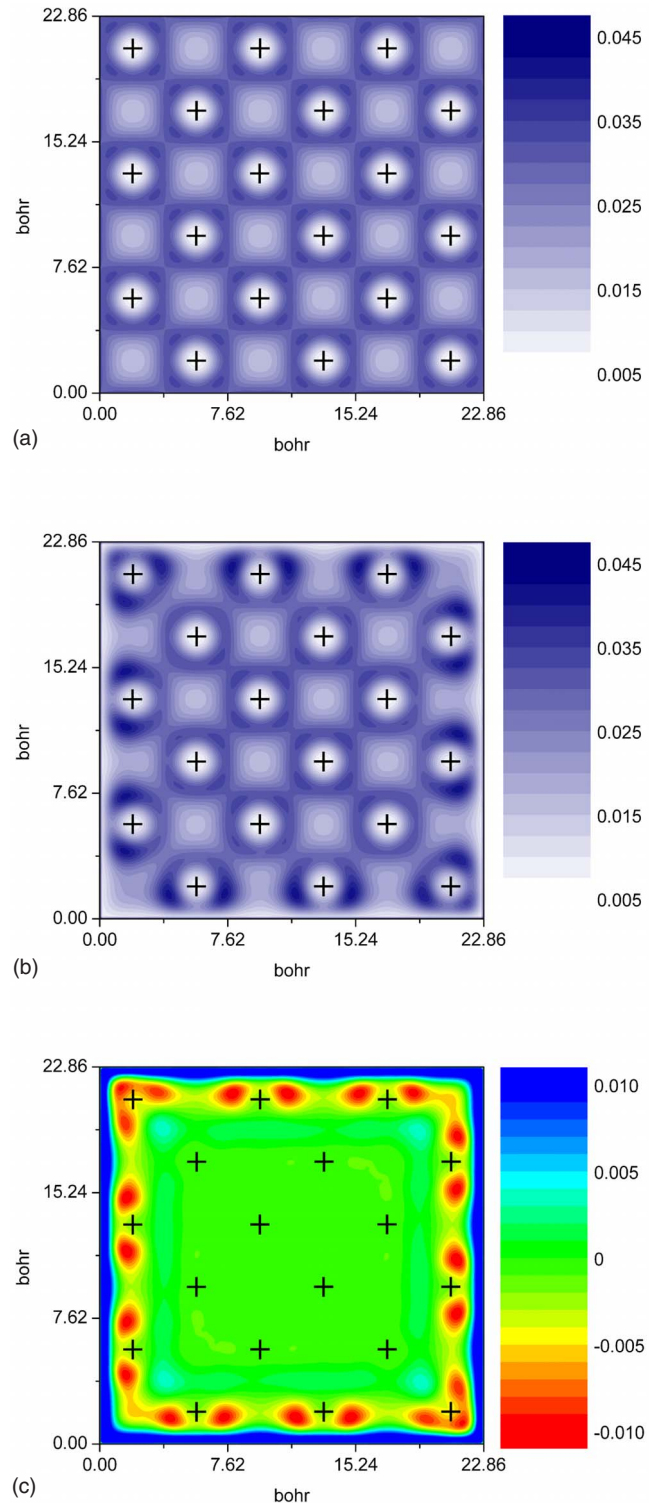

FIG. 6. (Color online) Periodic bulk fcc Al (a) initial guess and (b) optimized electron densities (number of electrons per cubic bohr) from a cut through an interior atomic plane of a 108-atom cluster using the WGC KEDF and second-order discretization under Dirichlet boundary conditions, with values at the boundary fixed at those optimum for bulk fcc Al. (c) Difference between the electron densities of (a) and (b). Nuclear positions (+) are marked for all in-plane Al nuclei.

implementation of the WGC KEDF under Dirichlet boundary conditions is consistent with its implementation under periodic boundary conditions. The small density mismatch near the edge of the cell in this test case is to be expected, since the nonlocal and long-range terms in OF-DFT (electrostatic and the WGC KEDF) require density data beyond the edge of the cell in order to reproduce the full periodic density. Larger clusters can be expected to recover the bulk electron density from the KEDF as the distance from the interior atoms to the boundaries increases, but such studies require a parallel version of PROFESS that makes more efficient use of memory. Alternatively, an embedding or padding atom approach can be taken to allow the nonlocal, long-range terms to be accounted for correctly up to the edge of the system of interest.[22]

V. SUMMARY AND CONCLUSIONS

In this paper, we have demonstrated how the nonlocal, double-density-dependent WGC functional can be derived analytically under periodic boundary conditions by directly solving the second-order differential equation for the terms in the WGC kernel. We have also shown how the WGC KEDF can be implemented under Dirichlet boundary conditions without resorting to approximations of the WGC kernel.

We validated our implementation of the WGC KEDF under Dirichlet boundary conditions by comparing to the same system under periodic boundary conditions with respect to a single aluminum atom and a 14-atom cluster of aluminum atoms. However, in order to interrogate large isolated systems, an efficient parallel implementation of the program is needed, since 14-atom clusters are the largest isolated clusters that can currently be studied on a single processor with 4 Gbytes of memory.

In isolated clusters, a large part of the system necessarily consists of vacuum so that the electron density may decay naturally to zero at the boundaries. This adds great cost to the calculation. However, an embedded system with nonzero boundary conditions requires no such vacuum region, allowing up to 108 atoms to be studied. Thus, we demonstrated the ability of the WGC KEDF to handle nonzero values at the boundaries (deriving the boundary conditions from a periodic calculation) by studying a 108-atom cluster of aluminum atoms. This ability to properly handle nonzero boundary conditions will be necessary if OF-DFT is to be incorporated into a multiscale model that explicitly resolves the solution down to atoms in regions that require it.

*Corresponding author.

[1] G. S. Ho, V. Lignères, and E. A. Carter (unpublished).

[2] W. Kohn and L. J. Sham, Phys. Rev. **140**, A1133 (1965).

[3] Y. A. Wang and E. A. Carter, in *Theoretical Methods in Condensed Phase Chemistry*, Progress in Theoretical Chemistry and Physics, edited by S. D. Schwartz (Kluwer, New York, 2000).

[4] Y. A. Wang, N. Govind, and E. A. Carter, Phys. Rev. B **60**, 16350 (1999); **64**, 089903(E) (2001).

[5] B. Zhou, V. Lignères, and E. A. Carter, J. Chem. Phys. **122**, 044103 (2005).

[6] L.-W. Wang and M. P. Teter, Phys. Rev. B **45**, 13196 (1992).

[7] F. Perrot, J. Phys.: Condens. Matter **6**, 431 (1994).

[8] M. Pearson, E. Smargiassi, and P. A. Madden, J. Phys.: Condens. Matter **5**, 3221 (1993).

[9] E. Smargiassi and P. A. Madden, Phys. Rev. B **49**, 5220 (1994).

[10] M. Foley and P. A. Madden, Phys. Rev. B **53**, 10589 (1996).

[11] Y. A. Wang, N. Govind, and E. A. Carter, Phys. Rev. B **58**, 13465 (1998); **64**, 129901(E) (2001).

[12] B. Zhou and E. A. Carter, J. Chem. Phys. **122**, 184108 (2005).

[13] J. Lindhard, K. Dan. Vidensk. Selsk. Mat. Fys. Medd. **28**, 8 (1954).

[14] C. J. García-Cervera, Comm. Comp. Phys. **2**, 334 (2007).

[15] R. W. Hockney and J. W. Eastwood, *Computer Simulation Using Particles* (Adam Hilger, New York, 1988).

[16] L.-W. Wang and M. P. Teter, Phys. Rev. B **45**, 13196 (1992).

[17] V. Lignères and E. A. Carter (unpublished).

[18] G. B. Arfken and H. J. Weber, *Mathematical Methods for Physicists*, 5th ed. (Harcourt, San Diego, CA/Academic, New York, 2001).

[19] D. M. Ceperley and B. J. Alder, Phys. Rev. Lett. **45**, 566 (1980).

[20] J. P. Perdew and A. Zunger, Phys. Rev. B **23**, 5048 (1981).

[21] G. S. Ho, Ph.D. thesis, Princeton University, 2008.

[22] X. Zhang and G. Lu, Phys. Rev. B **76**, 245111 (2007).